Int. J. Heat Mass Transfer. Vol. 36, No. 4, pp. 1073–1083, 1993
Printed in Great Britain

0017–9310/93 $6.00 + 0.00

A new analytic technique for 3-D heat transfer from a cylinder with two or more axially interacting eccentrically embedded vessels with application to countercurrent blood flow

Y. L. WU, S. WEINBAUM and L. M. JIJI
Department of Mechanical Engineering, The City College of the City University of New York, New York, NY 10031, U.S.A.

(*Received* 31 *July* 1991 *and in final form* 15 *January* 1992)

Abstract—A new approximate analytic solution technique is developed for treating the heat exchange between two or more axially interacting vessels which are eccentrically embedded in a cylinder. The cylinder exchanges heat by convection with the environment and has a non-uniform surface temperature due to the vessel eccentricity. The flow in the vessels can be either countercurrent or unidirectional. The solution is constructed by superposition of a new solution for a single embedded vessel which exactly satisfies the boundary conditions when the thermal conductivity of the fluid is equal to that of the cylinder material and is a very good approximation when these conductivities are not equal. Comparison with an exact solution for a single embedded vessel, when the conductivities are not equal, shows that the approximate solution results in very minor errors for a wide range of the governing parameters. As an application of the new technique the two-vessel solution is used to examine the countercurrent heat exchange in a human arm.

1. INTRODUCTION

THIS STUDY was motivated by the need to describe the heat exchange between the thermally significant countercurrent arteries and veins which occur throughout the macro- and microvasculature of humans and animals. This three-way energy exchange occurs, for example, in the major axial arteries and veins that supply and drain the human limbs, fingers, and the rat's tail. A basic heat transfer model for such systems is a countercurrent artery–vein pair which is eccentrically embedded in a cylinder with surface convection to the environment (Fig. 1). The eccentricity is arbitrary since the artery–vein pair may be close to the center of the tissue cylinder or the surface.

Although the motivation and focus in this study is the modeling of the biological systems described above, the analysis is equally applicable to heat transfer in engineering systems such as buried pipes and solar collectors.

Previous studies [1–7] have analyzed heat transfer problems for one or two vessels embedded in infinite, semi-infinite or finite cylindrical media. Various boundary conditions on the vessels and cylinder surfaces were examined. Chato [1] considered two unequal vessels at uniform surface temperatures embedded in an infinite medium. Wissler [2] treated the same configuration with continuity of heat flux and non-uniform vessel wall temperature and was able to obtain an exact solution for the case of a linear thermal gradient with equal vessel and medium conductivities.

The problem of a single vessel in a semi-infinite medium was examined by Chato [1] and Bau and Sadhal [3]. The free surface exchanges heat by convection with the environment in ref. [1] and is isothermal in ref. [3].

Defelice and Bau [4] analyzed a single vessel which is eccentrically embedded in a cylinder using a conformal mapping method. The boundary conditions on the vessel and cylinder surfaces were of the third kind, i.e. convective.

Recent interest in modeling countercurrent vessels in perfused tissue and limbs has motivated studies on two vessels embedded in a cylinder. Baish *et al.* [5] considered two equal vessels symmetrically placed in a cylinder. Vessel boundary conditions were of the

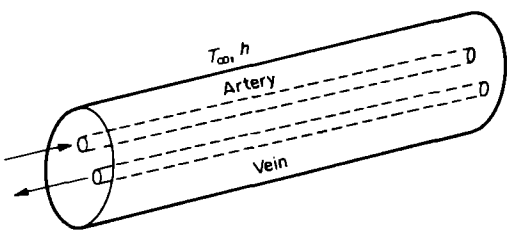

FIG. 1. Schematic of countercurrent vessels embedded in a cylinder.

NOMENCLATURE

a	vessel radius (a, v)
a_n	coefficients for single vessel non-conformal mapping solution, defined by equation (13)
A_n, B_n, C_n	numerical coefficients for bicylindrical solution in equations (31) and (32)
b_n, c_n	coefficients for countercurrent solutions, defined by equation (45)
Bi	Biot number, hR/k_t
c	specific heat
h	heat transfer coefficient
k	thermal conductivity
$\bar{k}$	ratio of fluid to embedding medium thermal conductivities
Nu	Nusselt number of vessel, hR/k_f
Pe	Peclet number of vessel, $2\rho_f c_f a_a V_a/k_f$
q	heat flow rate per unit length of the vessel
r	radial coordinate, Fig. 2
R	radius of embedding cylinder, Fig. 2
s	distance from origin to vessel axis, Fig. 2
sp	axis-to-axis distance between vessels, Fig. 2
T	temperature
T_0	artery bulk temperature at $z = 0$
T_∞	ambient temperature
x, y	Cartesian coordinates, Fig. 3
V	mean fluid flow velocity
$\bar{V}$	ratio of V_v to V_a
z	dimensionless axial coordinate
Z	axial coordinate.

Greek symbols

α, β	bicylindrical coordinates, Fig. 3
θ	dimensionless temperature
θ_{tm}	dimensionless tissue mean temperature
λ_i	eigenvalue defined by equation (54)
η, ξ	defined by equations (55) and (56)
ρ	dimensionless radial coordinate
ρ_f	density of fluid in vessels
ρ_R	dimensionless radius of embedding cylinder
σ_a	shape factor for single vessel case, defined by equation (19)
σ_{av}	shape factor between vessels, defined by equation (57)
σ_m	shape factor between vessel pair and environment, defined by equation (58)
ϕ	polar angle in cylindrical coordinate shown in Fig. 2
χ_i	constant defined by equations (52) and (53)
ω_{ij}	component of eigenvector, defined by equations (52) and (53).

Superscript

$^-$	dimensionless.

Subscripts

a	vessel for single vessel case artery for countercurrent flow case
b	bulk
f	fluid in vessels
h	homogeneous temperature
m	matrix value for vessels and embedding cylinder
p	particular temperature
t	tissue
v	vein
w	wall.

third kind, while the cylinder surface was at a uniform temperature. A similar problem was solved by Zhu *et al.* [6] using unequal vessels at uniform but unequal surface temperatures.

Since the major axial countercurrent artery–vein pairs in human limbs are eccentrically located, Zhu *et al.* [7] investigated the effect of eccentricity of two unequal vessels which are asymmetrically embedded near the center of a cylinder. They imposed a convective condition on the cylinder surface and satisfied continuity of temperature and heat flux at the vessels' surfaces. A perturbation solution was obtained which is limited to small eccentricity of the artery–vein pair. This is a serious limitation in the biological applications mentioned earlier since the eccentricity can be significant, with the major axial countercurrent artery–vein pairs running much closer to the surface than the center of the limb, finger or tail.

This paper removes this limitation by constructing a new approximate solution for a single vessel with arbitrary eccentricity. This solution is then applied to two unequal countercurrent vessels arbitrarily embedded in a cylinder which is subjected to the general boundary conditions treated in Zhu *et al.* [7]. The solution is approximate because it exactly satisfies the continuity of the heat flux condition at the vessel surface only when the ratio of fluid to the embedding material conductivity, $\bar{k}$, is unity.

A solution to the multiple embedded vessel problem may be obtained by the superposition of the single vessel solutions provided the basic solutions for each vessel satisfy the continuity of temperature and flux at the surfaces of the other vessels and their superposition satisfies the surface boundary condition on the embedding cylinder. Although conformal mapping can be used to treat the single vessel case, as in ref. [4], the form of the solution precludes superposition. The difficulty is traced to the nature of the

boundary conditions considered, since solutions to two or more individual vessels in a cylinder cannot be transformed to common bicylindrical coordinates. An alternative approach is developed here in which a new non-conformal mapping solution for an individual vessel is constructed in which superposition methods can be applied.

The effect of not exactly satisfying the continuity of the heat flux condition at the vessel's surface when $\bar{k} \neq 1$ is investigated by first obtaining a new exact solution for a single vessel in a cylinder with surface convection, which is valid for any value of $\bar{k}$, and comparing the predictions of this new exact solution with the approximate solution. The results show that the discrepancy is remarkably small over a wide range of the three governing parameters: the cylinder Biot number, the eccentricity and the cylinder–vessel diameter ratio.

2. FORMULATION

Consider two or more flow vessels embedded in a cylinder with surface convection. The geometry of the cross-sectional plane and the coordinate system used in the analysis are illustrated in Fig. 2, in which two countercurrent vessels are shown. We assume that the flow in the vessels is laminar with a parabolic velocity profile with mean velocities V_a and V_v. The Peclet number is assumed to be very large and the cylinder is long. Thus axial conduction and end effects can be neglected.

The non-dimensional parameters and variables which are appropriate for both the single embedded vessel case and the countercurrent flow case illustrated in Fig. 2 are defined as follows:

$$\bar{a}_v = \frac{a_v}{a_a}, \quad \overline{sp} = \frac{sp}{a_a}, \quad \bar{s}_a = \frac{s_a}{a_a}$$

$$\bar{s}_v = \frac{s_v}{a_a}, \quad \rho = \frac{r}{a_a}, \quad \rho_R = \frac{R}{a_a}, \quad \rho_a = \frac{r_a}{a_a}$$

$$\rho_v = \frac{r_v}{a_v}, \quad Bi = \frac{hR}{k_t}, \quad p_e = \frac{2\rho_f c_f a_a V_a}{k_f}$$

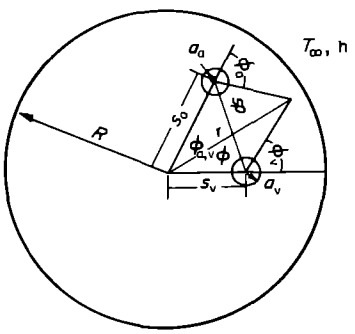

FIG. 2. The geometry of the cross-sectional plane and coordinate system.

$$\bar{k} = \frac{k_f}{k_t}, \quad \bar{V} = \frac{V_v}{V_a}, \quad z = \frac{Z}{a_a p_e}, \quad \theta = \frac{T - T_z}{T_0 - T_z}.$$

The subscripts a and v have been used here to denote an artery–vein pair that will be used as a simple model for the arm later in the paper. The technique, however, can be applied to any number of parallel vessels with flow in either direction. Based on the above assumptions and definitions the dimensionless energy equations for the artery and vein are:

$$\frac{1}{\rho}\frac{\partial}{\partial\rho}\left(\rho\frac{\partial\theta_a}{\partial\rho}\right) + \frac{1}{\rho^2}\frac{\partial^2\theta_a}{\partial\phi^2} = (1-\rho_a^2)\frac{\partial\theta_a}{\partial z}$$

$$\text{for} \quad \rho_a < 1 \quad (1)$$

$$\frac{1}{\rho}\frac{\partial}{\partial\rho}\left(\rho\frac{\partial\theta_v}{\partial\rho}\right) + \frac{1}{\rho^2}\frac{\partial^2\theta_v}{\partial\phi^2} = -\bar{V}(1-\rho_v^2)\frac{\partial\theta_v}{\partial z}$$

$$\text{for} \quad \rho_v < 1. \quad (2)$$

The minus sign in (2) is used to describe countercurrent flow for the biological application. The heat conduction equation in the surrounding tissue cylinder is

$$\frac{1}{\rho}\frac{\partial}{\partial\rho}\left(\rho\frac{\partial\theta_t}{\partial\rho}\right) + \frac{1}{\rho^2}\frac{\partial^2\theta_t}{\partial\phi^2} = 0$$

$$\text{for} \quad \rho_a \geqslant 1, \rho_v \geqslant 1. \quad (3)$$

The corresponding boundary conditions are

$$\theta_{a,v} = \theta_t \qquad \text{for } \rho_{a,v} = 1 \qquad (4)$$

$$\bar{k}\frac{\partial\theta_{a,v}}{\partial\rho_{a,v}} = \frac{\partial\theta_t}{\partial\rho_{a,v}} \qquad \text{for } \rho_{a,v} = 1 \qquad (5)$$

$$\frac{\partial\theta_t}{\partial\rho} = -\frac{Bi}{\rho_R}\theta_t \qquad \text{for } \rho = \rho_R. \qquad (6)$$

In order to separate the variables in equations (1) and (2), we assume that the convection terms $\partial\theta_{a,v}/\partial z$ can be approximated by the axial gradient of the bulk temperatures in the vessels, $d\theta_{ab,vb}/dz$. Conservation of the axial energy flux in the vessels leads to the following expression for the vessel:

$$\theta_{ab,vb} = \frac{2}{\pi}\int_0^{2\pi}\int_0^1 \theta_{a,v}(1-\rho_{a,v}^2)\rho_{a,v}\,d\rho_{a,v}\,d\phi_{a,v}. \quad (7)$$

Introducing this approximation into equations (1)–(3), we obtain

$$\nabla^2\theta_a = (1-\rho_a^2)\frac{d\theta_{ab}}{dz} \qquad \text{for } \rho_a < 1 \qquad (8)$$

$$\nabla^2\theta_v = -\bar{V}(1-\rho_v^2)\frac{d\theta_{vb}}{dz} \qquad \text{for } \rho_v < 1 \qquad (9)$$

$$\nabla^2\theta_t = 0 \qquad \text{for } \rho_a \geqslant 1, \rho_v \geqslant 1 \qquad (10)$$

where the Laplacian operator is used to describe the conduction terms.

3. SINGLE VESSEL SOLUTION

In this section, two solutions for the single vessel case are presented: a non-conformal mapping analytic solution which is exact only when $\bar{k} = 1$ and a bicylindrical solution based on conformal mapping which is valid for all values of $\bar{k}$. The former will be used in a superposition scheme to construct the solution for two or more vessels while the latter will be used to examine the accuracy of the approximate solution when $\bar{k} \neq 1$. The geometry of the cross-sectional plane and the bicylindrical coordinates for the single vessel analysis are illustrated in Fig. 3.

3.1. *Non-conformal mapping solution*

The governing equations for the vessel and embedded material (tissue) are given in (8) and (10) respectively. The corresponding boundary conditions are equations (4)–(6). The temperature solution can be decomposed into two parts $\theta = \theta_h + \theta_p$, where θ_h is the homogeneous solution and θ_p is the particular solution. The particular solutions for the vessel and tissue are:

$$\theta_{pa} = \left(\frac{1}{4}\rho_a^2 - \frac{1}{16}\rho_a^4 - \frac{3}{16}\right)\frac{d\theta_{ab}}{dz} \quad \rho_a < 1 \qquad (11)$$

$$\theta_{pt} = \tfrac{1}{4}\bar{k}(\ln \rho_a)\frac{d\theta_{ab}}{dz} \quad \rho_a \geqslant 1 \qquad (12)$$

and the homogeneous solution for the tissue, θ_h, takes the form

$$\theta_{ht} = \left(a_0 + \sum_{n=1}^{\infty} a_n \rho^n \cos n\phi\right)\frac{d\theta_{ab}}{dz}. \qquad (13)$$

Before adding the particular solution for the tissue (12) to the homogeneous solution (13), they must first be expressed in terms of common coordinates. Transforming the coordinates ρ_a, ϕ_a in the particular solution to ρ, ϕ and combining the resulting equation with the tissue homogeneous solution (13), we obtain

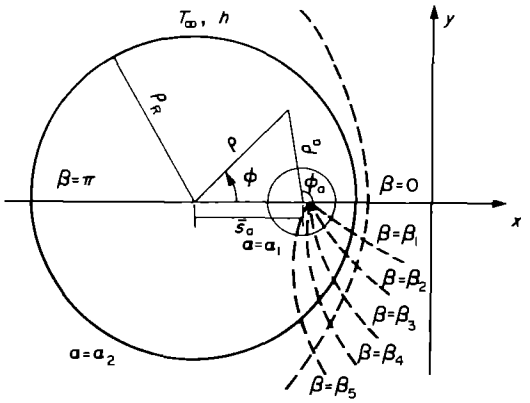

FIG. 3. Radial coordinate and bicylindrical coordinate system for a single vessel.

$$\theta_t = \left(a_0 + \sum_{n=1}^{\infty} a_n \rho^n \cos n\phi\right)\frac{d\theta_{ab}}{dz} + \tfrac{1}{8}\bar{k}\ln(\rho^2 + \bar{s}_a^2 - 2\rho\bar{s}_a\cos\phi)\frac{d\theta_{ab}}{dz}. \qquad (14)$$

The coefficients a_0 and a_n in (14) are determined from boundary condition (6); however, their evaluation is not straightforward. Equation (14) is substituted in (6) and integral expressions for a_n are then obtained from orthogonality. These integrals can be converted into contour integrals in the complex plane and then evaluated using residue theory. This elegant analysis, which is described in the Appendix, leads to the expressions

$$a_0 = -\frac{\bar{k}}{4}\left(\frac{1}{Bi} + \ln \rho_R\right) \qquad (15)$$

$$a_n = \frac{\bar{k}}{4(n+Bi)\rho_R^n}\left(\frac{Bi}{n} - 1\right)\left(\frac{\bar{s}_a}{\rho_R}\right)^n. \qquad (16)$$

A homogeneous solution to the vessel equation (8) is also required to satisfy boundary condition (5). A series solution of the form (13) cannot be used for $\bar{k} \neq 1$ since there is a singularity in the vessel region $\rho_a \leqslant 1$. Although an alternative infinite series solution can be constructed, the determination of the coefficients in this infinite series would require a cumbersome numerical evaluation. However, one notes that if $\bar{k} = 1$ the solution (13) will satisfy boundary conditions (4) and (5) and the vessel equation (8) exactly. When $\bar{k} \neq 1$, the homogeneous solution (13) satisfies boundary condition (4), but not (5) and the solution (14) is only approximate, but, nevertheless, as we shall show shortly, highly accurate for most conditions of interest. This approximate analytic solution to the single vessel–tissue problem given by (14), (15) and (16) can be superposed to construct the solution to two or more vessels embedded at any location in a cylinder. The error due to this approximation for $\bar{k} \neq 1$ is examined in detail in Section 5. Our approximate solution to the vessel temperature is thus obtained by adding (11) and (13)

$$\theta_a = \left(a_0 + \sum_{n=1}^{\infty} a_n \rho^n \cos n\phi\right)\frac{d\theta_{ab}}{dz} + \left(\frac{1}{4}\rho_a^2 - \frac{1}{16}\rho_a^4 - \frac{3}{16}\right)\frac{d\theta_{ab}}{dz}. \qquad (17)$$

Equations (14) and (17) reduce to the exact solutions for the limiting case $s_a = 0$.

To complete the analysis, the bulk temperature θ_{ab}, shape factor σ_a and Nusselt number Nu_a are needed. Substituting (17) into (7) and evaluating the double integrals, we obtain an expression relating θ_{ab} and its gradient:

$$\theta_{ab} = \left(-\frac{11}{96} + a_0 + \sum_{n=1}^{\infty} a_n \bar{s}_a^n\right)\frac{d\theta_{ab}}{dz}. \qquad (18)$$

The shape factor, σ_a, for heat transfer between the vessel and tissue cylinder is defined as:

$$\sigma_a = \frac{q_a}{2\pi k_t (T_{ab} - T_z)} = -\frac{\bar{k}}{4}\frac{\mathrm{d}\theta_{ab}}{\theta_{ab}} \quad (19)$$

where q_a is the heat transfer per unit length of vessel which is equal to $-\rho_t c_t \pi a_a^2 \bar{V}_a (\mathrm{d}T_{ab}/\mathrm{d}Z)$. Equations (18) and (19) yield

$$\sigma_a = \left(\frac{11}{24} - 4\sum_{n=0}^{\infty} a_n \bar{s}_a^n\right)^{-1}. \quad (20)$$

The Nusselt number for the vessel is defined as

$$Nu_a = \frac{q_a}{\pi k_t (T_{ab} - T_{aw})} = -\frac{1}{2}\frac{\mathrm{d}\theta_{ab}}{\theta_{ab} - \theta_{aw}} \quad (21)$$

where θ_{aw} is the dimensionless mean wall temperature of the vessel which is defined as

$$\theta_{aw} = \frac{1}{2\pi}\int_0^{2\pi} \theta_a(1, \phi_a)\,\mathrm{d}\phi_a \quad \text{at} \quad \rho_a = 1. \quad (22)$$

Substituting (17) into (22) and introducing the resulting expression for θ_{aw} into (21) we obtain

$$Nu_a = 48/11. \quad (23)$$

This result for the vessel Nusselt number is identical to that for a fully developed temperature distribution in a tube with constant surface heat flux. Examination of the vessel solution shows that the homogeneous part plays no role in the determination of the Nusselt number.

3.2. *Conformal bicircular mapping solution for a single vessel for* $\bar{k} \neq 1$

The single vessel solution presented above does not satisfy boundary condition (5) exactly when $\bar{k} \neq 1$. To examine the accuracy of this approximate solution an exact solution, valid for all values of $\bar{k}$, is developed in this section.

We introduce the bicylindrical transformation

$$x - iy = -\sinh \alpha_1 \tanh\left(\frac{\alpha + i\beta}{2}\right)$$

$$0 < \alpha < \infty, \quad -\pi < \beta < \pi \quad (24)$$

where the coordinates α, β are shown in Fig. 3. Constant α-coordinates are circles described by

$$(x + \sinh \alpha_1 \coth \alpha)^2 + y^2 = \frac{\sinh^2 \alpha_1}{\sinh^2 \alpha} \quad (25)$$

with α_1 representing the vessel and α_2 the cylinder. Geometric relationships require that

$$\frac{a_a}{R} = \frac{\sinh \alpha_2}{\sinh \alpha_1} \quad (26)$$

and

$$\bar{s}_a = \sinh \alpha_1 (\coth \alpha_2 - \coth \alpha_1). \quad (27)$$

The governing equations for the vessel and tissue in the new coordinates are the same as (8) and (10) with the Laplacian terms expressed in terms of α and β.

The boundary conditions transform to

$$(\cosh \alpha_2 + \cos \beta)\frac{\partial \theta_t}{\partial \alpha} = \sinh \alpha_2\, Bi\, \theta_t \quad \text{for } \alpha = \alpha_2 \quad (28)$$

$$\theta_a(\alpha, \beta) = \theta_t(\alpha, \beta) \quad \text{for } \alpha = \alpha_1 \quad (29)$$

and

$$\bar{k}\frac{\partial \theta_a}{\partial \alpha} = \frac{\partial \theta_t}{\partial \alpha} \quad \text{for } \alpha = \alpha_1. \quad (30)$$

The solution to the vessel equation (8) is

$$\theta_a = \left(c_0 + \sum_{n=1}^{\infty} c_n\, \mathrm{e}^{-n\alpha} \cos n\beta\right)\frac{\mathrm{d}\theta_{ab}}{\mathrm{d}z} + \left(\frac{1}{4}\rho_a^2 - \frac{1}{16}\rho_a^4 - \frac{3}{16}\right)\frac{\mathrm{d}\theta_{ab}}{\mathrm{d}z} \quad (31)$$

and the solution to the tissue equation (10) is

$$\theta_t = \left[\sum_{n=0}^{\infty} (A_n \sinh n\alpha + B_n \cosh n\alpha)\cos n\beta + A_0\alpha\right]\frac{\mathrm{d}\theta_{ab}}{\mathrm{d}z}. \quad (32)$$

The coefficients A_n, B_n, C_n are evaluated using boundary conditions (28)–(30). Boundary condition (28) yields a set of linear algebraic equations:

$$A_0(\cosh \alpha_2 - \alpha_2\, Bi \sinh \alpha_2) + \tfrac{1}{2}(A_1 \cosh \alpha_2 + B_1 \sinh \alpha_2) - B_0\, Bi \sinh \alpha_2 = 0 \quad (33)$$

$$A_0 + A_1(\cosh^2 \alpha_2 - Bi \sinh^2 \alpha_2) + A_2 \cosh 2\alpha_2 + B_1(\cosh \alpha_2 \sinh \alpha_2 - Bi \sinh \alpha_2 \cosh \alpha_2) + B_2 \sinh 2\alpha_2 = 0 \quad (34)$$

and

$$A_{n-1}(\cosh \alpha_2 - \tanh n\alpha_2 \sinh \alpha_2)\frac{n-1}{2} + A_n(n \cosh \alpha_2 - Bi \sinh \alpha_2 \tanh n\alpha_2) + A_{n+1}(\cosh \alpha_2 + \tanh n\alpha_2 \sinh \alpha_2)\frac{n+1}{2} + B_{n-1}(\tanh n\alpha_2 \cosh \alpha_2 - \sinh \alpha_2)\frac{n-1}{2} + B_n(n \cosh \alpha_2 \tanh n\alpha_2 - Bi \sinh \alpha_2) + B_{n+1}(\tanh n\alpha_2 \cosh \alpha_2 + \sinh \alpha_2)\frac{n+1}{2} = 0$$

$$\text{for } n \geqslant 2. \quad (35)$$

Boundary condition equation (29) requires that

$$c_0 = A_0\alpha_1 + B_0 \tag{36}$$

and

$$c_n = e^{n\alpha_1}(A_n \sinh n\alpha_1 + B_n \cosh n\alpha_1) \quad \text{for } n \geqslant 1. \tag{37}$$

Applying boundary condition equation (30), using orthogonality and evaluating the resulting integrals using residue theory, we obtain

$$A_0 = -\tfrac{1}{4}\bar{k} \tag{38}$$

and

$$c_n = \frac{1}{2n}(-1)^{n+1} - \frac{1}{k}e^{n\alpha_1}(A_n \cosh n\alpha_1 + B_n \sinh n\alpha_1) \quad \text{for } n \geqslant 1. \tag{39}$$

Equations (33)–(39) contain $3N+3$ unknowns, whereas the number of equations is $3N+2$. This set of equations is, therefore, not closed. Fortunately, $C_n \exp(-n\alpha_1)$ decreases as n is increased and thus it can be truncated at N terms. If we require that $C_{N+1}\exp(-(N+1)\alpha_1) = 0$, then the above equations can be truncated and solved in closed form. Computations for $C_{N+1}\exp(-(N+1)\alpha_1)$ show that it decreases very rapidly. The criterion used to choose N in the sequence is

$$\left|\frac{A_j^{N+1} - A_j^N}{A_j^{N+1}}\right| + \left|\frac{B_j^{N+1} - B_j^N}{B_j^{N+1}}\right| + \left|\frac{C_j^{N+1} - C_j^N}{C_j^{N+1}}\right| \leqslant 10^{-5} \quad \text{for } 0 \leqslant j \leqslant 10. \tag{40}$$

Using (19) as the definition for the shape factor, one obtains from (31)

$$\sigma_a = \left(\frac{11}{24} - 4\sum_{n=0}^{\infty}(-1)^n C_n e^{-2n\alpha_1}\right)^{-1}. \tag{41}$$

Result (41) is derived from a contour integration in the complex plane and residue theory. The Nusselt number for the vessel is again a constant equal to 48/11. This is the same as the value obtained from the approximate solution. This is not surprising since the homogeneous solution does not contribute to the Nusselt number.

4. TWO-VESSEL SOLUTION: COUNTERCURRENT HEAT EXCHANGE

As an example of the superposition solution for multiple vessels, consider the problem of two embedded vessels with counterflow heat exchange. The solution to this problem is obtained by superposition of two single vessel solutions presented in Section 3.1. The governing equations and boundary conditions are given by equations (4)–(6) and (8)–(10). The temperature solution is decomposed into two parts $\theta = \theta_h + \theta_p$, where θ_h and θ_p are the homogeneous and particular solutions, respectively. The particular solutions for the artery, vein and tissue are:

$$\theta_{pa} = \left(\frac{1}{4} - \rho_a^2 - \frac{1}{16}\rho_a^4 - \frac{3}{16}\right)\frac{d\theta_{ab}}{dz} - \bar{V}\bar{a}_v^2\left(\frac{1}{4}\bar{k}\ln\rho_v\right)\frac{d\theta_{vb}}{dz} \tag{42}$$

$$\theta_{pv} = \left(\frac{1}{4}\bar{k}\ln\rho_a\right)\frac{d\theta_{ab}}{dz} - \bar{V}\bar{a}_v^2\left(\frac{1}{4}\rho_v^2 - \frac{1}{16}\rho_v^4 - \frac{3}{16}\right)\frac{d\theta_{vb}}{dz} \tag{43}$$

$$\theta_{pt} = \left(\frac{1}{4}\bar{k}\ln\rho_a\right)\frac{d\theta_{ab}}{dz} - \bar{V}\bar{a}_v^2\left(\frac{1}{4}\bar{k}\ln\rho_v\right)\frac{d\theta_{vb}}{dz}. \tag{44}$$

The homogeneous solution in the three regions that replaces (13), (15) and (16) is

$$\theta_h = \left(b_0 + \sum_{n=1}^{\infty} b_n\rho^n\cos n(\phi - \phi_{av})\right)\frac{d\theta_{ab}}{dz} + \left(c_0 + \sum_{n=1}^{\infty} c_n\rho^n\cos n\phi\right)\bar{V}\bar{a}_v^2\frac{d\theta_{vb}}{dz} \tag{45}$$

where

$$b_0 = -\frac{\bar{k}}{4}\left(\frac{1}{Bi} + \ln\rho_R\right), \tag{46}$$

$$b_n = \frac{\bar{k}}{4(n+Bi)\rho_R^N}\left(\frac{Bi}{n} - 1\right)\left(\frac{\bar{s}_a}{\rho_R}\right)^n, \tag{47}$$

$$c_0 = \frac{\bar{k}}{4}\left(\frac{1}{Bi} + \ln\frac{\rho_R}{a_v}\right), \tag{48}$$

and

$$c_n = -\frac{\bar{k}}{4(n+Bi)\rho_R^N}\left(\frac{Bi}{n} - 1\right)\left(\frac{\bar{s}_v}{\rho_R}\right)^n. \tag{49}$$

The temperature solutions in the artery and vein are used to determine the relationships for the bulk temperatures as defined by equation (7). The evaluation procedure of these double integrals is the same as that used in the single vessel case. Thus, the bulk temperature relationships for the interacting vessels that replace (18) for a single vessel are

$$\theta_{ab} = \left(\sum_{n=0}^{\infty} b_n\bar{s}_a^n - \frac{11}{96}\right)\frac{d\theta_{ab}}{dz} + \left(\sum_{n=0}^{\infty} c_n\bar{s}_a^n - \frac{\bar{k}\ln\left(\frac{\bar{sp}}{a_v}\right)}{4}\right)\bar{V}\bar{a}_v^2\frac{d\theta_{vb}}{dz} \tag{50}$$

$$\theta_{vb} = \left(\sum_{n=0}^{\infty} b_n\bar{s}_v^n + \frac{\bar{k}\ln\bar{sp}}{4}\right)\frac{d\theta_{ab}}{dz} + \left(\sum_{n=0}^{\infty} c_n\bar{s}_v^n + \frac{11}{96}\right)\bar{V}\bar{a}_v^2\frac{d\theta_{vb}}{dz}. \tag{51}$$

The coupled equations (50) and (51) can be solved analytically if a_v, $\bar{V}$, $\bar{s}_a$, $\bar{s}_v$ and $\overline{sp}$ are constant:

$$\theta_{ab} = \chi_1\omega_{11}\exp(\lambda_1 z) + \chi_2\omega_{12}\exp(\lambda_2 z) \quad (52)$$

$$\theta_{vb} = \chi_1\omega_{21}\exp(\lambda_1 z) + \chi_2\omega_{22}\exp(\lambda_2 z) \quad (53)$$

where eigenvalues $\lambda_{1,2}$ are given by

$$\lambda_{1,2} = \frac{-\eta \pm \sqrt{(\eta^2 - \xi)}}{\xi} \quad (54)$$

where

$$\xi = \bar{V}\bar{a}_v^2\left(\sum_{n=0}^{r} b_n\bar{s}_a^n - \frac{11}{96}\right)\left(\sum_{n=0}^{r} c_n\bar{s}_v^n + \frac{11}{96}\right) - \bar{V}\bar{a}_v^2\left(\sum_{n=0}^{r} b_n\bar{s}_v^n + \frac{\bar{k}\ln\overline{sp}}{4}\right) \times\left(\sum_{n=0}^{r} c_n\bar{s}_a^n - \frac{\bar{k}\ln\left(\frac{\overline{sp}}{a_v}\right)}{4}\right) \quad (55)$$

and

$$\eta = -\frac{1}{2}\left(\left(\sum_{n=0}^{r} b_n\bar{s}_a^n - \frac{11}{96}\right) + \bar{V}\bar{a}_v^2\left(\sum_{n=0}^{r} c_n\bar{s}_v^n + \frac{11}{96}\right)\right). \quad (56)$$

ω_{ij} are the eigenvector coefficients in equations (50) and (51) and χ_1 and χ_2 are integral constants which are determined by the bulk temperature at a reference position. For three or more vessels, relationships for θ_{bi}, $i = 1, 2, 3, \ldots, N$, analogous to (50) and (51) would be obtained.

5. RESULTS AND DISCUSSION

5.1. *Accuracy of the approximate solution: single embedded vessel*

Since boundary condition (5) is satisfied exactly only when the thermal conductivity ratio $\bar{k}$ is equal to unity, the solutions (14) and (17) are approximate for all other values of $\bar{k}$. In this section we evaluate the error associated with this approximation by considering the single embedded vessel case for which an exact solution has been obtained in Section 3.2 using conformal mapping. In particular, the shape factor σ_a is examined by evaluating the ratio of our approximate solution for σ_a, equation (20), with our exact solution for σ_a, equation (41). Comparisons are made for a wide range of the four governing parameters: the conductivity ratio $\bar{k}$, Biot number Bi, eccentricity $\bar{s}_a$ and the cylinder–vessel radius ratio ρ_R. The effect of conductivity ratio and Biot number on the accuracy of the shape factor for a configuration with large eccentricity defined by $\rho_R = 5$ and $\bar{s}_a = 3.5$ is shown in Fig. 4. Three Biot numbers are considered:

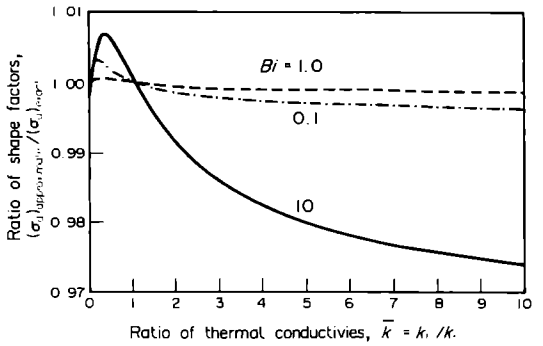

FIG. 4. Effect of conductivity ratio $\bar{k}$ on the accuracy of the single vessel shape factor. Comparison between approximate and exact (conformal mapping) results for $\rho_R = 5$ and $\bar{s}_a = 3.5$.

$Bi = 0.1$, 1.0, and 10. Values of Bi typical of the human upper limbs are 1.5 in air and 10 in water. The conductivity ratio is varied from 0 to 10. Since the approximate solution is exact for $\bar{k} = 1$, all curves intersect at a point corresponding to a shape factor ratio, $(\sigma_a)_{approximate}/(\sigma_a)_{exact}$, of unity. For Biot numbers of 0.1 and 1.0, the error in the shape factor is insignificant and at $Bi = 10$ and $\bar{k} = 10$ the error is less than 3%. For blood vessels in tissue $1 \leqslant \bar{k} < 2$ and in engineering applications $\bar{k}$ ranges from 6×10^{-5} (air–copper) to 12 (water–85% magnesia insulation). Figure 4 also shows that for $\bar{k} \leqslant 1$ the error in shape factor is less than 1%. This latter range of $\bar{k}$ includes fluids such as air, water and oil flowing through cylinders of materials such as glass, wood, metal, etc., which are common engineering applications.

The effect of eccentricity and Biot number on the accuracy of shape factor for $\bar{k} = 10$ and $\rho_R = 5$ is shown in Fig. 5. For the limiting case of concentric cylinders, i.e. $\bar{s}_a = 0$, the exact result for the shape factor ratio of unity is obtained for all Biot numbers regardless of the value of $\bar{k}$, since equations (14) and (17) reduce to the exact solutions. As the eccentricity is increased the error increases monotonically, reaching 7% at $\bar{s}_a = 3.99$ for $Bi = 10$ but remaining small (less than 1%) for $Bi = 0.1$ and 1.0. It should be noted that

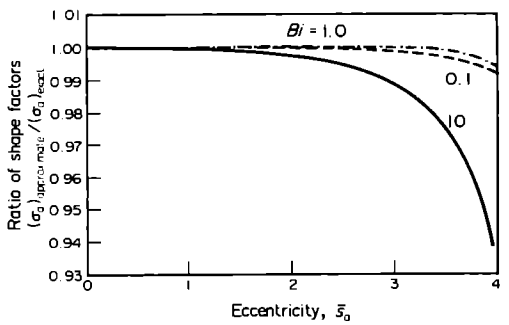

FIG. 5. Effect of eccentricity $\bar{s}_a$ on the accuracy of the single vessel shape factor. Comparison between approximate and exact (conformal mapping) results for $\rho_R = 5$ and $\bar{k} = 10$.

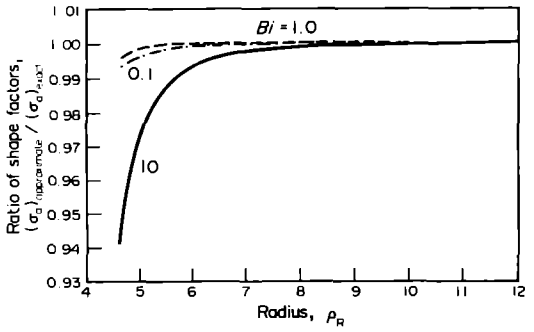

FIG. 6. Effect of cylinder size ρ_R on the accuracy of the single vessel shape factor. Comparison between approximate and exact (conformal mapping) results for $\bar{s}_a = 3.5$ and $\bar{k} = 10$.

the maximum eccentricity for $\rho_R = 5$ is 4.0, which corresponds to a vessel which is at a tangent to a cylinder. The effect of the cylinder–vessel diameter ratio ρ_R on the shape factor ratio for $\bar{k} = 10$ and $\bar{s}_a = 3.5$ is shown in Fig. 6. Here the error in the shape factor increases as the cylinder radius ρ_R is decreased. Since $\bar{s}_a$ is constant, a decrease in ρ_R has the effect of increasing the eccentricity. The minimum value of ρ_R representing the tangent configuration is obtained when $\rho_R = 4.5$. On the other hand, at large ρ_R ($\rho_R \geqslant 12$), the limiting case of concentric cylinders is approached and an exact value for the shape factor is obtained for all values of Bi and $\bar{k}$.

The results shown in Figs. 4–6 indicate that even though boundary condition (5) is not satisfied exactly when $\bar{k} \neq 1$, the error associated with this approximation is minor, especially for Bi or $\bar{k}$ less than unity. In particular, in biological applications where the value of $\bar{k}$ is approximately equal to unity, the error is indeed insignificant.

5.2. *Two embedded vessels*

The two-vessel solution is used to examine the Nusselt number, the artery–vein and matrix shape factors, the axial vessel bulk temperature distribution, the axial mean cylinder temperature distribution, and the surface temperature distribution of the artery, vein and cylinder.

Following the same procedure as for a single vessel, the Nusselt number for both artery and vein is found to be 48/11.

The two-vessel solution is used to obtain two heat transfer shape factors, σ_{av} and σ_m, which describe, respectively, the heat transfer rate between the two vessels, and that between the vessel–tissue matrix and the environment. These factors are defined as

$$\sigma_{av} = \frac{q_a - q_v}{\pi k_t (T_{ab} - T_{vb})} \tag{57}$$

and

$$\sigma_m = \frac{q_a + q_v}{\pi k_m (T_m - T_z)} \tag{58}$$

where T_m is the mean matrix temperature (artery, vein and cylinder) given by

$$\frac{T_m - T_z}{T_0 - T_z} = \theta_m = \frac{1}{\pi \rho_R^2} \int_0^{\rho_R} \int_0^{2\pi} \theta(\rho, \phi) \rho \, d\rho \, d\phi \tag{59}$$

and k_m is the matrix conductivity given by

$$k_m = \frac{1 + \bar{a}_v^2}{\rho_R^2} k_t + \left(1 - \frac{1 + \bar{a}_v^2}{\rho_R^2}\right) k_t. \tag{60}$$

Substituting the solutions for the bulk temperature of the artery and vein, (50) and (51), into the definition of σ_{av}, we obtain

$$\sigma_{av} = \frac{-\frac{1}{2}\bar{k}\left(\frac{d\theta_{ab}}{dz} + \bar{V}\bar{a}_v^2 \frac{d\theta_{vb}}{dz}\right)}{\left[\sum_{n=0}^{\infty} b_n(\bar{s}_a^n - \bar{s}_v^n) - \frac{11}{96} - \frac{\bar{k}}{4}\ln \bar{sp}\right]\frac{d\theta_{ab}}{dz} + \left[\sum_{n=0}^{\infty} c_n(\bar{s}_a^n - \bar{s}_v^n) - \frac{\bar{k}}{4}\ln\left(\frac{\bar{sp}}{\bar{a}_v}\right) - \frac{11}{96}\right]\bar{V}\bar{a}_v^2 \frac{d\theta_{vb}}{dz}}. \tag{61}$$

For the general case, σ_{av} depends on the local axial gradients of the vessel bulk temperatures. However, for the special case of two equal radii vessels embedded at equi-distance from the center of a cylinder, i.e. $\bar{a}_v = 1$ and $\bar{s}_a = \bar{s}_v$, (61) simplifies to

$$\sigma_{av} = \frac{2\bar{k}}{\frac{11}{24} + \bar{k}\ln \bar{sp}}. \tag{62}$$

This result shows that the shape factor σ_{av} for this special case depends only on the distance between the two vessels $\bar{sp}$ and is independent of eccentricity. It is interesting to note that if the radius of the embedding medium cylinder is infinite, then $\bar{s}_a$ is equal to $\bar{s}_v$. Setting $\bar{s}_a = \bar{s}_v$ and assuming equal flow rates in the two vessels, i.e. $\bar{V}\bar{a}_v^2 = 1$, equation (61) reduces to Wissler's [2] results for two vessels embedded in an infinite medium. Result (62), without the $\ln \bar{sp}$ term, was also obtained to leading order in the perturbation of Zhu *et al.* [7] for small eccentricity. Expression (62) is especially useful in biological applications involving extremities such as a finger or tail where the artery–vein pair is symmetrically located relative to the skin surface.

Using the temperature solutions for the artery, vein and tissue to determine T_m from (59) and substituting the result into the definition of σ_m, we obtain

$$\sigma_m = \frac{4\left(\frac{d\theta_{ab}}{dz} - \bar{V}\bar{a}_v^2 \frac{d\theta_{vb}}{dz}\right)\frac{\rho_R^2}{(1 + \bar{a}_v^2)\bar{k} + (\rho_R^2 - 1 - a_v^2)}}{\left[\frac{Bi+2}{Bi} - \left(\frac{\bar{s}_a}{\rho_R}\right)^2 - \left(\frac{1}{\rho_R}\right)^2 + \frac{2}{3\bar{k}\rho_R^2}\right]\frac{d\theta_{ab}}{dz} - \left[\frac{Bi+2}{Bi} - \left(\frac{\bar{s}_v}{\rho_R}\right)^2 - \left(\frac{\bar{a}_v}{\rho_R}\right)^2 + \frac{2}{3\bar{k}}\left(\frac{\bar{a}_v}{\rho_R}\right)^2\right]\bar{V}\bar{a}_v^2 \frac{d\theta_{vb}}{dz}}. \tag{63}$$

Since the vessel area is small compared with the embedding medium area, the term $(1/\rho_R)^2$ in (63) is negligible. For $\bar{s}_a = \bar{s}_v$ and $\bar{k} \simeq 1$ (63) simplifies to

$$\sigma_m = \frac{4}{\dfrac{Bi+2}{Bi} - \left(\dfrac{\bar{s}_a}{\rho_R}\right)^2}. \tag{64}$$

The dependence of the shape factor σ_m on $\bar{s}_a/\rho_R$ for various Biot numbers (0.1, 1.0, 10) is shown in Fig. 7. For $Bi < 1$, the matrix shape factor is essentially constant independent of the vessels' location in the cylinder. However, at $Bi = 10$, σ_m increases sharply as the vessels move closer to the cylinder surface. When the eccentricity is small, $\bar{s}_a/\rho_R \ll 1$, expression (64) reduces to the perturbation solution of Zhu *et al.* [7], in which the $(\bar{s}_a/\rho_R)^2$ term does not appear.

Finally, the two-vessel solution is applied to the human arm to determine the artery–vein and matrix shape factors and the bulk and surface temperature distribution of the artery, vein and arm. The configuration examined models the arm as a constant radius $\rho_R = 12$. The artery and vein are assumed to be symmetrically embedded in the tissue cylinder at $\bar{s}_a = \bar{s}_v = 8$ with $\overline{sp} = 3$ and $\bar{a}_v = 1$. The conductivity ratio $\bar{k}$ is equal to unity and thus boundary condition (5) is satisfied exactly. Using (62) the artery–vein shape factor σ_{av} is found to be 1.28.

From (64), the corresponding matrix shape factors σ_m at Biot numbers of 0.1, 1 and 10 for this model of the arm are 0.195, 1.565 and 5.294, respectively.

To determine the axial variation of bulk temperatures and the distribution of surface temperatures, it is necessary to first specify the boundary conditions on the bulk temperatures. Two conditions are needed to evaluate the constants of integration in (50) and (51). From the definition of the dimensionless artery bulk temperature, θ_{ab}, the first boundary condition is

$$\theta_{ab} = 1, \quad z = 0 \tag{65}$$

where $z = 0$ is the shoulder end of the arm. The second boundary condition is obtained from the experimental data of Bazett *et al.* [8], who measured the median basilic vein temperature at two ambient air temperatures of 21 and 34.5°C. Thus:

$$\theta_{vb} = 0.56, \quad Z/L = 0.22 \quad \text{at} \quad T_\infty = 21^\circ\text{C} \tag{66a}$$

$$\theta_{vb} = 0.15, \quad Z/L = 0.22 \quad \text{at} \quad T_\infty = 34.5^\circ\text{C}. \tag{66b}$$

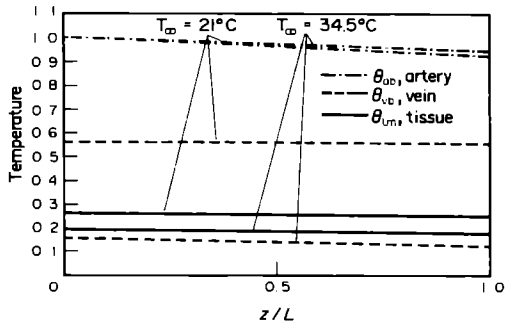

FIG. 8. Effect of environment temperature on the axial variation of the artery and vein bulk temperature and the tissue mean temperature for countercurrent heat exchange for $\rho_R = 12, \bar{s}_a = \bar{s}_v = 8, \overline{sp} = 3, \bar{V} = 1, \bar{a}_v = 1, \bar{k} = 1, Pe = 3500$ and $Bi = 1.48$.

These data are for the arm at rest where the Peclet number at the shoulder is approximately 3500 at normal ambient temperatures. The Biot number, which accounts for both convection and radiation, is 1.48. Based on boundary conditions (65) and (66), the results for the axial variation of the artery, vein and tissue temperatures, θ_{ab}, θ_{vb} and θ_{tm}, are shown in Fig. 8 for both ambient temperatures. The monotonic variation of these temperatures along the arm is unrealistic due to the simplified model used, which neglects three key factors: cross-sectional area variation of the arm, the axial decrease in the Peclet number due to the bleed-off from the axial vessels to the muscle and cutaneous circulations and the enhancement in tissue conductivity due to blood perfusion, described by the Weinbaum–Jiji bioheat equation. Blood bleed-off from the artery acts to warm the arm towards the wrist. These factors can be accounted for following the theoretical approach developed in Song *et al.* [9] and Zhu [10].

Peripheral variations of surface temperature at $Z/L = 0.5$ for the artery, vein and arm at $T_\infty = 21$ and 34.5°C are shown in Figs. 9 and 10, respectively.

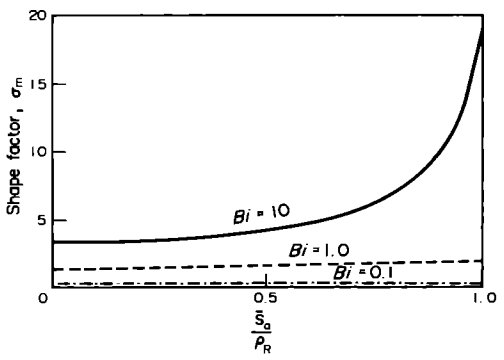

FIG. 7. Matrix shape factor for countercurrent vessels for $\bar{s}_a = \bar{s}_v$ and $\bar{k} \simeq 1$.

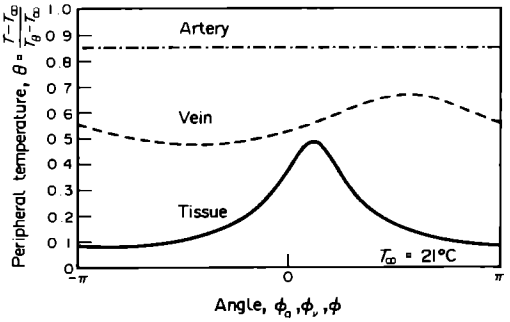

FIG. 9. Peripheral surface temperature variation for the artery, vein and arm at cross-section $Z/L = 0.5$, for $Bi = 1.48, \rho_R = 12, \bar{s}_a = \bar{s}_v = 8, \overline{sp} = 3, \bar{V} = 1, \bar{a}_v = 1, \bar{k} = 1$, $Pe = 3500$ and $T_\infty = 21$°C.

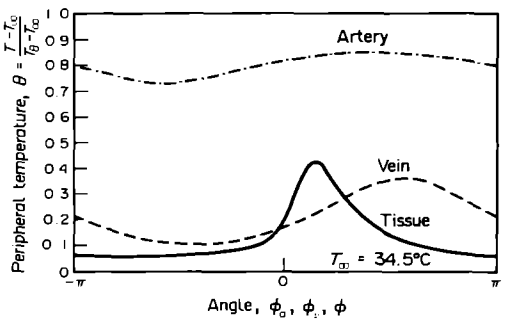

FIG. 10. Peripheral surface temperature variation for the artery, vein and arm at cross-section $Z/L = 0.5$, for $Bi = 1.48$, $\rho_R = 12$, $\bar{s}_a = \bar{s}_v = 8$, $\overline{sp} = 3$, $\bar{V} = 1$, $\bar{a}_v = 1$, $\bar{k} = 1$, $Pe = 3500$ and $T_\infty = 34.5$°C.

These plots show that peripheral variation of surface temperature is moderate for the artery and more pronounced for the vein and arm. At both ambient temperatures the arm surface temperature peaks in the vicinity of the artery–vein pair. This single peak form is due to the fact that the distance between the artery and vein is smaller than their distance from the arm surface and thus they act as a single source.

Although the artery loses heat to the tissue and vein at both ambient temperatures, heat interchange between tissue and vein is strongly influenced by the ambient temperature. Figure 9 shows that at $T_\infty = 21$°C the vein heats the tissue, while at $T_\infty = 34.5$°C (Fig. 10), the direction of heat flow is reversed along the vein circumference. Thus at a given section along the arm, heat can flow from the tissue to the vein and from the vein to the tissue along the vein periphery.

6. CONCLUDING REMARKS

(1) Although the continuity of the flux boundary condition at the vessel's surface is not exactly satisfied for $\bar{k} \neq 1$, the error in the new approximate analytic solution derived herein is small for a very wide range of $\bar{k}$ values. In biological applications where $\bar{k}$ is approximately equal to unity and in many engineering applications where $\bar{k} \leqslant 1$, the error in the solution is of the order of 1% or less. Although this conclusion is based on a detailed study of the single embedded vessel case, the error associated with two or more embedded vessels can be expected to be of the same order since the multi-vessel solution is constructed by superposition of single vessel solutions.

(2) The approximate solution presented in Section 4 for two vessels embedded anywhere in a cylinder can be readily extended to applications where the number of vessels is more than two. Indeed, this is the case in the human forearm, where the major artery–vein pair in the upper arm bifurcates at the elbow to form two countercurrent pairs.

(3) The assumption of constant artery, vein and arm cross-sectional areas used to obtain a solution for the axial temperature distribution in the simplified model for the arm in this paper can be relaxed. Axial variation of the three cross-sectional areas can be taken into consideration using a numerical integration of equations (50) and (51) along the length of the arm.

(4) With minor modification the method of solution can be applied to the case of two dissimilar fluids. Such applications are common in engineering systems.

Acknowledgements—This research was supported by NSF grant CBT-8702582 and NIH grant 5R01 HL2609.

REFERENCES

1. J. C. Chato, Heat transfer to blood vessels, *ASME J. Biomech. Engng* **102**, 110–118 (1980).
2. E. H. Wissler, An analytical solution for countercurrent heat transfer between parallel vessels with a linear axial temperature gradient, *ASME J. Biomech. Engng* **110**, 254–256 (1988).
3. H. H. Bau and S. S. Sadhal, Heat losses from a fluid flowing in a buried pipe, *Int. J. Heat Mass Transfer* **25**, 1621–1629 (1982).
4. R. F. Defelice, Jr. and H. H. Bau, Conductive heat transfer between eccentric cylinders with boundary conditions of the third kind, *ASME J. Heat Transfer* **105**, 678–680 (1983).
5. J. W. Baish, P. S. Ayyaswamy and K. R. Foster, Small-scale temperature fluctuations in perfused tissue during local hyperthermia, *ASME J. Biomech. Engng* **108**, 246–250 (1986).
6. M. Zhu, S. Weinbaum, L. M. Jiji and D. E. Lemons, On the generalization of the Weinbaum–Jiji bioheat equation to microvessels of unequal size: the relation between the near field and local average tissue temperatures, *ASME J. Biomech. Engng* **110**, 74–81 (1988).
7. M. Zhu, S. Weinbaum and L. M. Jiji, Heat exchange between unequal countercurrent vessels asymmetrically embedded in a cylinder with surface convection, *Int. J. Heat Mass Transfer* **33**, 2275–2284 (1990).
8. H. C. Bazett, L. Love, M. Newton, L. Eisenberg, R. Day and R. Forster II, Temperature changes in blood flowing in arteries and veins in man, *J. Physiol.* **1**, 3–19 (1948).
9. W. J. Song, S. Weinbaum, L. M. Jiji and D. E. Lemons, A combined macro and microvascular model for whole limb heat transfer, *ASME J. Biomech. Engng* **110**, 259–268 (1987).
10. M. Zhu, Generalization of the Weinbaum–Jiji bioheat equation and studies of whole limb heat transfer. Ph.D. Dissertation, The City University of New York, New York (1990).

APPENDIX

The purpose of this Appendix is to show how the coefficients a_0 and a_n in equation (14) can be analytically evaluated. Substituting (14) into boundary condition (6) yields

$$\sum_{n=1}^{\infty} a_n n \rho_R^{n-1} \cos n\phi + \frac{\bar{k}}{4} \frac{\rho_R - \bar{s}_a \cos\phi}{\rho_R^2 + \bar{s}_a^2 - 2\rho_R \bar{s}_a \cos\phi} - \frac{Bi}{\rho_R}\left(a_0 + \sum_{n=1}^{\infty} a_n \rho_R^n \cos n\phi + \frac{\bar{k}}{8} \ln(\rho_R^2 + \bar{s}_a^2 - 2\rho_R \bar{s}_a \cos\phi)\right). \quad \text{(A1)}$$

If (A1) is integrated over ϕ from 0 to 2π all the a_n terms vanish except a_0 and one obtains

$$a_0 = -\frac{\bar{k}}{4}\left(\frac{1}{Bi} + \ln \rho_R\right). \quad \text{(A2)}$$

If one multiplies equation (A1) by $\cos m\phi$ and then integrates term by term over the interval $0 \leqslant \phi \leqslant 2\pi$, one obtains for each of the terms on the right hand side of (A1)

$$\int_{-\pi}^{\pi} a_0 \cos m\phi \, d\phi = 0 \tag{A3}$$

$$\int_{-\pi}^{\pi} \left(\sum_{n=1}^{\infty} a_n n \rho_R^n \cos n\phi \right) \cos m\phi \, d\phi = m a_m \rho_R^m \pi \tag{A4}$$

and

$$\int_{-\pi}^{\pi} \frac{\bar{k}}{8} \ln (\rho_R^2 + \bar{s}_a^2 - 2\rho_a \bar{s}_a \cos \phi) \cos m\phi \, d\phi = -\frac{\bar{k} \rho_a \bar{s}_a}{4m} \int_{-\pi}^{\pi} \frac{\sin \phi \sin m\phi}{\rho_R^2 + \bar{s}_a^2 - 2\rho_R \bar{s}_a \cos \phi} d\phi \tag{A5}$$

where the right hand side of (A5) is obtained after integration by parts. We define the integral I_1 by

$$I_1 = \int_{-\pi}^{\pi} \frac{\sin \phi \cos m\phi}{\rho_R^2 + \bar{s}_a^2 - 2\rho_R \bar{s}_a \cos \phi} d\phi \tag{A6}$$

and denote the integral in (A5) by

$$I_2 = \int_{-\pi}^{\pi} \frac{\sin \phi \sin m\phi}{\rho_R^2 + \bar{s}_a^2 - 2\rho_R \bar{s}_a \cos \phi} d\phi \tag{A7}$$

so that their sum,

$$I_1 + iI_2 = \int_{-\pi}^{\pi} \frac{\sin \phi \, (\cos m\phi + i \sin m\phi)}{\rho_R^2 + \bar{s}_a^2 - 2\rho_R \bar{s}_a \cos \phi} d\phi, \tag{A8}$$

can be treated by a contour integration in the complex plane. Introducing the complex variable $\Omega = Re^{i\phi}$, when $d\phi = -i \, d\Omega/\Omega$ on the unit circle $R = 1$, the integral (A8) can be written as a contour integration around the unit circle in the complex plane:

$$I_1 + iI_2 = \oint \frac{1}{2\rho_R \bar{s}_a} \frac{(\Omega^2 - 1)\Omega^{m-1}}{\Omega^2 + \dfrac{\rho_R^2 + \bar{s}_a^2}{\rho_R + \bar{s}_a} \Omega + 1} d\Omega. \tag{A9}$$

Using residue theory, the integral (A9) can be evaluated as

$$I_1 + iI_2 = \frac{\pi i}{\rho_R \bar{s}_a} \left(\frac{\bar{s}_a}{\rho_R} \right)^m \tag{A10}$$

$$\int_{-\pi}^{\pi} \frac{\bar{k}}{8} \ln (\rho_R^2 + \bar{s}_a^2 - 2\rho_a \bar{s}_a \cos \phi) \cos m\phi \, d\phi = -\frac{\bar{k}\pi}{4m} \left(\frac{\bar{s}_a}{\rho_R} \right)^m. \tag{A11}$$

The integral obtained from the second term on the left hand side of (A1) can be evaluated by a similar procedure. The contour integration on the unit circle in the Ω plane in this case leads to

$$\int_{-\pi}^{\pi} \frac{\bar{k}}{4} \frac{\rho_R \bar{s}_a \cos \phi}{\rho_R^2 + \bar{s}_a^2 - 2\rho_R \bar{s}_a \cos \phi} \cos m\phi \, d\phi = \frac{\bar{k}\pi}{4\rho_R} \left(\frac{\bar{s}_a}{\rho_R} \right)^m. \tag{A12}$$

Combining results (A4), (A11), and (A12), one obtains the following expression for the coefficient a_n:

$$a_n = \frac{\bar{k}}{4(n + Bi)\rho_R^n} \left(\frac{Bi}{n} - 1 \right) \left(\frac{\bar{s}_a}{\rho_R} \right)^n. \tag{A13}$$